Raman spectroscopy of the paramagnetic spin flip in $Cd_{1-x}Mn_xTe$, the role of band-gap excitons as intermediate states, and optically detected electron-nuclear double resonance

J. Stühler, M. Hirsch, G. Schaack, and A. Waag
Physikalisches Institut der Universität Würzburg, D-97074 Würzburg, Federal Republic of Germany
(Received 5 October 1993)

We have studied the paramagnetic resonance signal (PRS, $\Delta m = +1$) of the $3d^5$ spin of Mn^{2+} in $Cd_{1-x}Mn_xTe$ epilayers and, less extensively, in a quantum-well structure by means of Raman spectroscopy in an external magnetic field of 6 T at low temperatures. The exciting laser or the scattered light were in resonance with electronic transitions (free exciton transitions) between the valence and the conduction band. The resonances have been observed by continuously tuning the wavelengths of the exciting dye laser in Voigt and Faraday backscattering geometries. For the off-resonance case the PRS is only expected in Voigt geometry with crossed polarizations of incident and scattered light (single resonance case, either ingoing or outcoming). Contrary to that, in resonance, the transition appears with large intensities as double resonances in the "forbidden" parallel polarizations and also in Faraday configuration. These results can be interpreted by considering a spin flip of a nucleus with $I \geq \frac{1}{2}$ (^{111}Cd, ^{113}Cd, ^{125}Te, ^{55}Mn) simultaneously with the reorientation of the electronic spin of the $3d$ shell.

I. INTRODUCTION

Semimagnetic semiconductors exhibit a number of fascinating magnetic phenomena, which at present find widespread interest.[1,2] Especially the $A^{II}_{1-x}Mn_xB^{VI}$ compounds have been investigated in great detail. Here the percentage $100x$ of the cations in the semiconducting II-VI compound of the cubic zinc-blende structure has been substituted by Mn ions, which with their half-filled $3d$ shell ($3d^5$) display a total spin of $S = 5/2$, $L = 0$ (^6S) in the ground state. The band gap E_0 of the material increases linearly with x, especially for $Cd_{1-x}Mn_xTe$ according to $E_0 = (1.606 + 1.592x)$ eV at $T = 2$ K. Due to the strong exchange interaction between the localized $3d$ states of Mn and the sp^3 valence- and conduction-band states the effective g factors of the latter are strongly enhanced, causing a giant Zeeman splitting of the band-edge states, a very large Faraday rotation, and, most interesting, the formation of bound magnetic polarons. At low x ($x \leq 0.15$) most of the Mn^{2+} ions are in the paramagnetic state. With increasing concentration clusters of antiferromagnetically coupled Mn^{2+} ions are formed and a spin glass state is encountered at low temperatures. In this spin glass phase magnonlike spin excitations are observed.

In the following we concentrate on the low-x case, where another magnetic excitation, the spin flip $\Delta m_S = +1$ of a single Mn^{2+} ion within the ^6S ground state, is observed. This signal shifts linearly with the magnetic field B, $g = 2$. It is the well known paramagnetic resonance signal (PRS, Fig. 1), which we have studied by means of Raman resonance spectroscopy. We have followed the integrated intensity of the PRS, which shows resonance with the laser excitation or the scattered radiation or both, due to electronic transitions near the band edge in the sample. This yields additional information on the energy levels near the band edge and on the interaction mechanism between the localized spins and the charge carriers in the valence band (VB) and conduction band (CB), i.e., the role of band gap excitons as intermediate states in the scattering process is emphasized.

In Fig. 2 we have schematically plotted the energies of the CB with Γ_6 symmetry and the Γ_8 VB states in an external magnetic field, which show the well known paramagnetic saturation following a Brillouin function.[2] Due to the large splittings the corresponding dipole transitions of these band-gap excitons can be separated clearly. As the band gap E_0 is smaller than the energy of the $^6A_1 \leftrightarrow {}^4T_1$ transitions in the $3d$ shell of the Mn^{2+} ions for the x values considered (Fig. 1), resonances observed

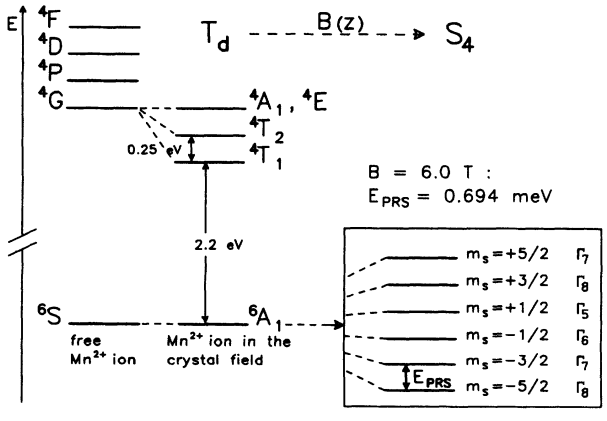

FIG. 1. Energy levels (schematic) of the $3d^5$ shell of Mn^{2+} in $Cd_{1-x}Mn_xTe$. The irreducible representations Γ_i are of the point group S_4 ($= T_d \otimes H_y$) (Ref. 5).

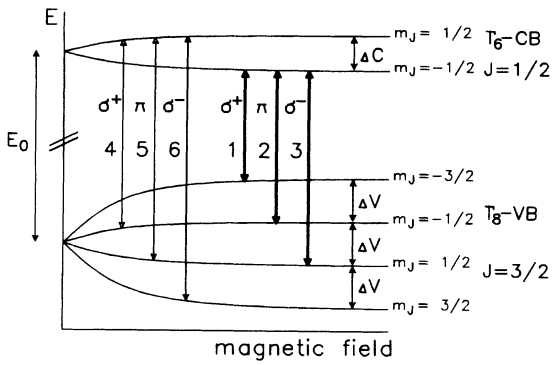

FIG. 2. The Γ_8 valence-band (VB) and the Γ_6 conduction-band (CB) states of $Cd_{1-x}Mn_xTe$, $x = 0.135$, in a magnetic field. $E_0 = 1.815$ eV, $\Delta V = 30$ meV, and $\Delta C = 21$ meV. The numbered arrows symbolize the electric dipole transitions with the polarizations indicated (see Figs. 5, 6, and 8).

in the spectral range of E_0 must be attributed to band-gap states. We have also investigated, although in less detail, the PRS in a quantum-well structure and give some preliminary results.

The PRS has already been observed previously by means of Raman spectroscopy.[3,4] Petrou *et al.*[3] suggested a Raman mechanism involving interband transitions in conjunction with the exchange interaction between band electrons and holes and the $3d$ electrons in Mn^{2+}. Our results fully support and prove this interpretation, but extend it to the nuclei in the lattice which display an angular momentum $\vec{I}$ ($I \geq 1/2$). Peterson *et al.*[4] have observed resonances of the PRS Raman signal at fixed wavelengths λ of the exciting laser but by varying temperature T and magnetic field B. We have observed Raman resonances at fixed T and B by varying λ over a broad range and using additional polarization geometries.

II. EXPERIMENTAL PROCEDURE

We have studied a molecular-beam epitaxy (MBE) grown, nominally undoped epilayer ($d = 1.6$ μm and $x = 0.135 \pm 0.01$ below the percolation limit, i.e., only Mn clusters of finite size exist) on a $Cd_{0.96}Zn_{0.04}Te$ substrate ([001]) which keeps the bidirectional stress in the layer as low as possible ($\frac{\Delta a}{a} = 0.03\,\%$). The spatial fluctuations Δx of x averaged over the size of the laser spot amount to $\Delta x \approx 0.001$. All measurements have been performed by immersion of the sample in liquid helium at $T = 1.85$ K in a split-coil magnet ($B \leq 7.5$ T) either in the Voigt or in the Faraday configuration. We used a dye laser (dye: DCM with two different sets of dielectric mirrors, tuning range 1.71 eV $\leq h\nu \leq$ 1.98 eV) with a prefilter monochromator, polarization optics, and cylindrical lenses to produce a line focus of $\approx 0.2 \times 3$ mm^2 on the sample in order to average over a larger sample area and to reduce sample heating, at the expense of a possibly increased linewidth due to the presence of a concentration gradient. Power densities of 1.0 W cm^{-2} on the sample surface have been applied, which result in a negligible local heating in the focus area of approximately 0.1 K. The scattered radiation has been analyzed using a computer controlled triple monochromator ($f = 50$ cm) equipped with an optical multichannel detector (OMD). The observed linewidth of the laser at 1.81 eV was 0.22 meV and the observed width of the PRS was 0.26 meV in all spectra at $B \geq 6$ T, corresponding to three channels of the OMD. No absorption corrections have been applied to the observed resonance profiles; the plotted cross sections are in arbitrary units only. They have been corrected, however, for the varying intensity of the laser and the spectral sensitivity of the spectrometer including its OMD. Circular polarization for varying wavelengths has been produced by applying a Soleil-Babinet compensator, while a quarter-wavelength plate in first order plus a linear polarizer has been used as an analyzer. The correct orientations of both have been controlled by the observation of circularly polarized luminescence according to Fig. 2.

The polarization selection rules for magnetic dipole Raman scattering can be obtained by the usual group-theoretical procedure: The point group of the zinc-blende structure is T_d, which is reduced to S_4 ($\bar{4}$) under application of a magnetic field $\vec{B}$ parallel to a cubic axis,[5] [notations of irreducible representations (IR) follow Ref. 5]. A magnetic dipole moment $\vec{R}$ ($\Delta m = \pm 1$) transforms, according to Γ_4 of T_d, to Γ_1 (R_z is antisymmetric), and Γ_3 and Γ_4 (R_x and R_y) of S_4 if $\vec{B} \parallel \vec{z}$. Quadrupolar transitions ($\Delta m = 0, \pm 2$) transform according to Γ_3 and Γ_5 (T_d) or to Γ_1 (symmetric), Γ_2, Γ_3, and Γ_4 of S_4. The representation of the ground-state multiplet of Mn^{2+} is spanned by the double group IR: Γ_5, Γ_6, $2\Gamma_7$, and $2\Gamma_8$ (Fig. 1), the transitions between neighboring levels, transform according to Γ_3 ($\Delta m = +1$) and Γ_4 ($\Delta m = -1$), according to Γ_2 for $\Delta m = \pm 2$, and, of course, to Γ_1 for $\Delta m = 0$. The $\Delta m = \pm 1$ transitions are thus observed in Raman scattering for the $-z(yx, xy)z$ orientation, where the direction of y is parallel to the external magnetic field and z is the growth direction of the epilayer, i.e., in a backscattering experiment only the Voigt geometry should be applicable for the observation of the PRS. The quadrupolar transitions ($\Delta m = 0, \pm 2$), which are forbidden in first order for magnetic dipole transitions, can be observed both in the Voigt geometry $\{-z(x,x)z$, $(\Gamma_1, \Delta m = 0)$ or $(\Gamma_2$, $\Delta m = \pm 2)$; $-z(y,y)z$, $(\Gamma_1)\}$ and in the Faraday geometry ($\vec{B} \parallel [001], z$) using circularly polarized radiation for the incoming and the outgoing radiation: $-z(\sigma^+, \sigma^+)z$ and $-z(\sigma^-, \sigma^-)z$, $(\Delta m = 0)$ or $-z(\sigma^+, \sigma^-)z$, $-z(\sigma^-, \sigma^+)z$, $(\Delta m = \pm 2)$.[6]

The usual selection rule

$$\frac{d\sigma}{d\omega} \sim |\vec{e}_B \times (\vec{e}_i \times \vec{e}_s)|^2 \qquad (1)$$

for Raman scattering at magnetic excitations in paramagnetic systems of isotropic or cubic symmetry[1,7] is in full accordance with the results above. Here σ is the scattering cross section and $\vec{e}_B$, $\vec{e}_i$, and $\vec{e}_s$ are the unit vectors of the static magnetic field and of the polarizations of the incident and the scattered radiation. For Raman backscattering experiments $\frac{d\sigma}{d\omega}$ is maximum for $\vec{e}_i \perp \vec{e}_s$ ("allowed" crossed polarization) and $\vec{e}_B$ in the

plane of the $Cd_{1-x}Mn_xTe$ layer (Voigt geometry). The parallel polarization ($\vec{e}_i \parallel \vec{e}_s$) is forbidden according to this rule, which states that one unit of angular momentum has to be transferred between the crystal and the radiation field for a single spin flip to occur. The Faraday geometry ($\vec{e}_B \perp \vec{e}_i, \vec{e}_s$) also results in $\frac{d\sigma}{d\omega} = 0$. In the Voigt orientation the light is π polarized if the E vector is oriented along y and σ polarized if it is along $x \parallel [100]$; it is always σ polarized in the Faraday orientation.[6,8] This selection rule is derived[7] assuming symmetry relations for the electric susceptibility of a magnetic material $[\chi^{ij}(\vec{M}) = \chi^{ji*}(\vec{M})]$, which are only valid in the nonresonance case. In the case of linear absorption of either the ingoing or outcoming radiation this rule (1) is severely violated and has to be replaced by the more general group-theoretical considerations given above.

III. EXPERIMENTAL RESULTS

In Fig. 3 we have plotted the Raman spectra taken at $B = 6$ T in crossed (σ, π) and parallel (π, π) polarizations. In both spectra we observe the LO phonons (Cd-like at 20.7 meV and Mn-like at 24.4 meV). The strong electronic spin-flip Raman line, which nearly coincides with the phonon at this magnetic field, appears at 21.0 meV only in (σ, π). Very close (0.695 meV Stokes shifted at $B = 6$ T) to the exciting laser near 1.81 eV (close to the band edge) the weak PRS is found, however, with non-negligible intensity also in the "forbidden" (π, π) polarization. A combination transition of the PRS with both phonons also occurs in both spectra. No additional structure near the PRS is observed due to the excitation of spin clusters (see below). The Raman line at $2\omega_{PRS}$, which was observed by Petrou *et al.*[3] and by Peterson *et al.*,[4] did not occur in our spectra with appreciable intensity for further evaluation.

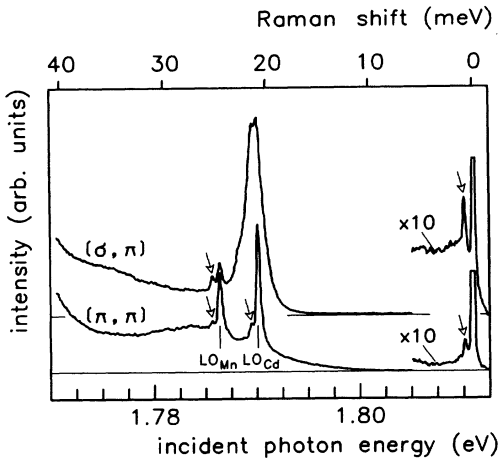

FIG. 3. Raman spectra of $Cd_{1-x}Mn_xTe$, $x = 0.135$ at $T = 1.6$ K, $B = 6$ T (Voigt geometry $\vec{B} \parallel [010]$), in crossed and parallel polarization of incoming and scattered light. Besides the LO phonons and the electronic spin flip, the paramagnetic resonance signal (arrows) and its combination with the phonons and luminescence transitions due to a spillover of the strong $1(\sigma)$ transition (< 1.78 eV) and the weak $2(\pi)$ transition (at 1.785 eV) are depicted. The zero intensity of the (σ, π) spectrum is shifted and marked by horizontal lines.

The linear Zeeman shift of the PRS with B has been determined from the combination of the Mn-like LO phonon with the PRS, because this combination can be followed to lower B values than the isolated PRS close to the Rayleigh line. The results have been plotted in Fig. 4. A g factor of 2.00 ± 0.10 is fitted to these data, which compares well with the more precise EPR value: $g = 2.010$.[9] The width of the PRS is determined by instrument resolution at all B values. These results agree with those of Rodriguez and Ramdas.[1] We did not observe a temperature dependence of g or of the width of the PRS as was reported in Ref. 10 for lower magnetic fields.

Figures 5 and 6 display the intensities of the PRS near the Rayleigh line as a function of the quantum energy of the exciting laser in the Voigt geometry for two orthogonal polarizations (Fig. 5) and for parallel polarizations (Fig. 6), normalized by the intensity of the incident radiation. Distinct extrema of the scattering cross section are found, which can be related to the various excitonic transitions indicated in Fig. 2 and which are marked by the arrows above the energy axes of Figs. 5 and 6. We have determined these excitonic transition energies by photoluminescence and photoluminescence excitation experiments and by resonance Raman experiments with the electronic spin flip. For the precise numbers we had to consider values for the exciton binding energy (≈ 3.7 meV) and its donor binding energy $[(D^0, X) \approx 3.7$ meV]. For details see Refs. 11 and 12. Figure 7 gives an example of the spectra and Raman resonances used to establish these energies.

In Fig. 8 the resonances for Faraday geometry are depicted. Here right and left circular polarization have been applied. Resonances are observed for identical polarizations (σ^+, σ^+) and (σ^-, σ^-), but not for orthogonal polarizations (σ^+, σ^-) or (σ^-, σ^+).[6] Spurious effects for the latter polarizations have to be attributed to the nonideal performance of the polarizer and analyzer and to the use of metallic mirrors at 45° incidence between sample and polarizer. The resonance enhancements and the halfwidths are comparable to the results found in the forbidden orientation above. The resonances in Fig. 8 are

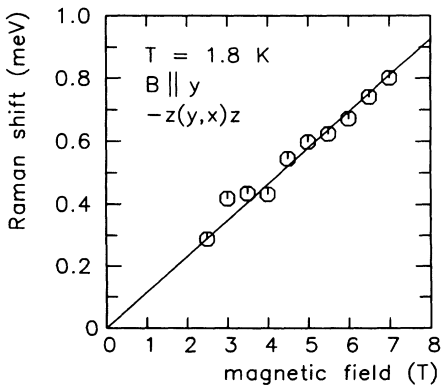

FIG. 4. Optically detected Zeeman shift of the PRS, $g = 2.00 \pm 0.10$.

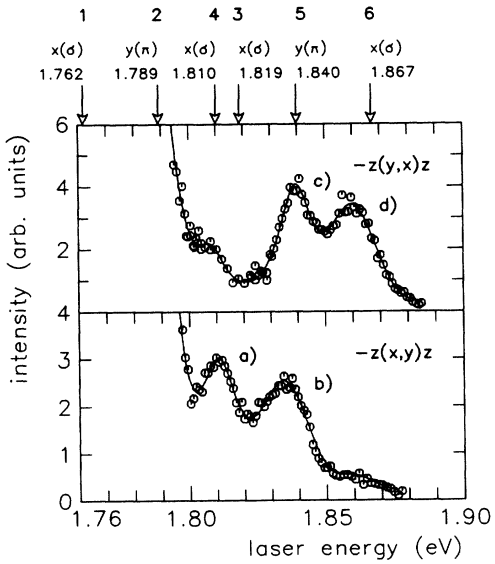

FIG. 5. Intensities of the PRS (Raman resonances) as a function of the exciting laser energies in allowed (crossed) polarizations at $B = 6$ T ($\vec{B} \parallel [010]$, in the epilayer), $T = 1.85$ K. The numbers, energies, and arrows on the top refer to the transitions indicated in Fig. 2. The lettering (a)–(d) corresponds to the different processes compiled in Table I. The observed Raman transitions are of Γ_3 type ($\triangle m_S = +1$).

interpreted as double resonances (see below).

The PRS phonon companions (Fig. 3) also show resonance behavior which coincides, however, with the resonances of the nearby phonon. Both resonance profiles in Fig. 5 show a strong increase when the laser approaches the intense band-edge luminescence (No. 1, and transition 1 in Fig. 2). No reliable measurements could be performed in this region because of the overlap of the

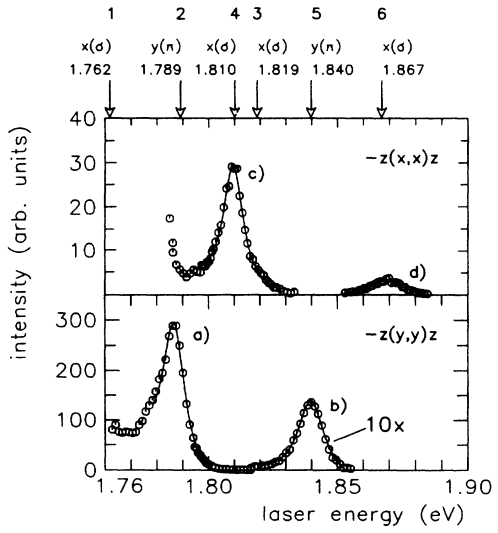

FIG. 6. Same as in Fig. 5, but in forbidden (parallel) polarizations, $\vec{B} \parallel [010]$. The observed Raman transitions are Γ_1 ($\triangle m = 0$) and Γ_2 ($\triangle m = \pm 2$) for the (xx) spectra and Γ_1 for the (yy) spectra. Note the change in scale at 1.815 eV in the $-z(yy)z$ spectrum. Between (a) and (b) the signal drops to ≈ 0.4 a.u. and virtually disappears between (c) and (d).

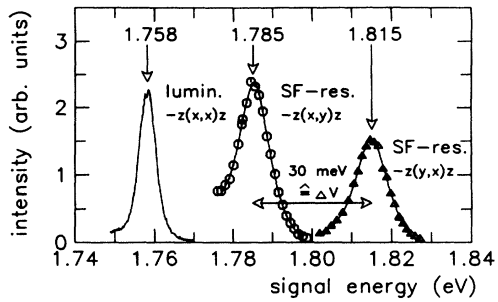

FIG. 7. Examples of the electronic spin-flip (SF) resonances in allowed polarizations ($x = 0.135$, $B = 6$ T, and $T = 1.85$ K); the energy difference $\triangle V$ equals the VB splitting of the light holes. Also plotted is the luminescence spectrum corresponding to transition $(1,\sigma)$ in Fig. 2. The energies of the dipole-allowed transitions 1, 2, and 3 (Fig. 2), as given in the top row here, differ slightly from the corresponding values found in Figs. 5 and 6 because of excitonic localization.

scattered and the spontaneously emitted light. This increase may be due to the increasing transparency of the crystal, i.e., the increase of the scattering volume, when the laser energy comes close to the band gap.

In the $-z(x,y)z$ polarization (lower part of Fig. 5) two distinct maxima [(a) and (b) at 1.811 and 1.834 eV] and a very weak one at 1.860 eV are observed. Resonance (a) is in good agreement with transition $(4,\sigma^+;|3/2,-1/2\rangle \leftrightarrow |1/2,1/2\rangle)$ (Fig. 2). Resonance (b) corresponds to $(5,\pi;|3/2,1/2\rangle \leftrightarrow |1/2,1/2\rangle)$, although there remains an energy difference of 5.5 meV. No other plausible identification of this transition exists, however. The resonance at 1.860 eV could be attributed to transition $(6,\sigma^-;|3/2,3/2\rangle \leftrightarrow |1/2,1/2\rangle)$. However,

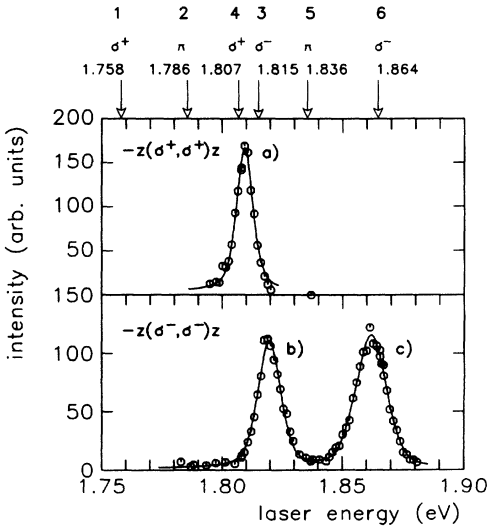

FIG. 8. PRS resonances in the Faraday configuration $\vec{B} \parallel [001]$. $B = 6$ T and $T = 1.6$ K. The x value differs slightly from the previous sample. σ^+ and σ^- are right and left circularly polarized light. The (σ^+,σ^+) and (σ^-,σ^-) transitions are of Γ_1 type ($\triangle m_S = 0$).

a spillover from the forbidden polarization $-z(x,x)z$ (see below) is more probable. The strong increase towards lower energies can be identified with transition $(1,\sigma^+;|3/2,-3/2\rangle \leftrightarrow |1/2,-1/2\rangle)$. Again the distinct increase with decreasing laser energies may be due to the increasing transparency of the crystal. It should be taken into account that the amplitudes of the cross sections given in Figs. 5 and 6 for different polarizations can only be compared qualitatively (i.e., with rather large error bars) for various experimental reasons (see below).

The orthogonal polarization $-z(y,x)z$ (upper part of Fig. 5) also displays three maxima: two are clearly resolved [(*c*) at 1.839 eV and (*d*) at 1.860 eV] and a weak shoulder at 1.807 eV. (*c*) can obviously again be identified with $(5,\pi;|3/2,1/2\rangle \leftrightarrow |1/2,1/2\rangle)$. Resonance (*d*) is related to $(6,\sigma^-;|3/2,3/2\rangle \leftrightarrow |1/2,1/2\rangle)$; there is, however, a distinct energy difference close to 7 meV. (*d*) is not well defined and riding as a shoulder on the descent of (*c*). The weak shoulder (1.807 eV) might be identified with $(4,\sigma^+;|3/2,-1/2\rangle \leftrightarrow |1/2,1/2\rangle)$; however, a spillover from $-z(x,x)z$ is again more probable. The half widths of these resonances are on the average rather large (14 − 19 meV; see Table I). Between the resonances the scattered intensity remains finite.

In the Voigt geometry in the forbidden (parallel) polarization directions the same g factor of the PRS is observed as above within experimental limits. Surprisingly there exist very clear resonances (Fig. 6), with clean polarization properties, i.e., no spillover is observed beyond experimental uncertainties. The half widths of the resonances are reduced as compared to the allowed polarizations to about 2/3 of the previous values (Table I), while the maxima of the scattered intensities have attained values more than one order of magnitude larger than in the allowed spectra. (The vertical scales of Figs. 5 and 6 can only be compared with some caution as the laser-illuminated spots on the sample surface are not necessarily identical in both spectra after polarization reversal.)

TABLE I. Resonances of the Raman scattering cross sections for crossed (allowed) and parallel (forbidden) polarizations in the Voigt configuration ($\vec{B} \parallel [010]$) and in the Faraday configuration ($\vec{B} \parallel [001]$). Shown is a comparison between observed frequencies and values calculated from observed excitonic transitions. e and h are scattering mechanisms (Figs. 10 and 11) with a virtual spin flip of an electron or hole, respectively; FWHM denotes full width at half maximum. The resonance intensities are in arbitrary units (arb.); these data have not been corrected for sample absorption or for change of polarization.

	Voigt configuration			
Polarization	$-z(x,y)z$		$-z(y,x)z$	
Resonance (Fig. 5)	(*a*)	(*b*)	(*c*)	(*d*)
Dipole transition (Fig. 2)	4	5	5	6
Type of resonance	incoming	outgoing	incoming	outgoing
Scattering	α,β	β	δ,ϵ	ϵ
Mechanism (Fig. 10)	e,h	h	e,h	h
Observed position (eV)	1.811	1.834	1.839	1.860
FWHM of resonance (eV)	0.017	0.019	0.014	0.019
Intensity (arb.)	2.4	2.0	3.7	2.9
Calculated position of resonance (eV)	1.810	1.840	1.840	1.867
Polarization	$-z(y,y)z$		$-z(x,x)z$	
Resonance (Fig. 6)	(*a*)	(*b*)	(*c*)	(*d*)
Dipole transition (Fig. 2)	2	5	4	6
Type of resonance	double	double	double	double
Scattering mechanism (Fig. 11)	$\approx \alpha,\beta,\gamma$	$\approx \alpha,\beta,\gamma$	α,β,γ	$\approx \alpha,\gamma$
Observed position (eV)	1.786	1.839	1.809	1.868
FWHM of resonance (eV)	0.009	0.012	0.009	0.014
Intensity (arb.)	247	15	26	3.0
Calculated position of resonance (eV)	1.789	1.840	1.810	1.867
	Faraday configuration			
Polarization	$-z(\sigma^+,\sigma^+)z$		$-z(\sigma^-,\sigma^-)z$	
Resonance (Fig. 8)	(*a*)		(*b*)	(*c*)
Dipole transition (Fig. 2)	4	(1)[a]	3	6
Type of resonance	double		double	double
Scattering mechanism (Fig. 11)	α,β,γ		$\approx \alpha,\beta,\gamma$	$\approx \alpha,\gamma$
Observed position (eV)	1.809		1.819	1.861
FWHM of resonance (eV)	0.008		0.011	0.015
Intensity (arb.)	163		108	113
Calculated position of resonance (eV)	1.807		1.815	1.864

[a]Transition 1 is not detectable due to band-edge luminescence.

In between two resonances the signal is usually very low, much lower than for the crossed spectra, i.e., *the selection rule (1) is obviously obeyed for the off-resonance case, but seriously violated in resonance.* In this case the selection rules for the absorption or emission of single quanta (incoming or outgoing resonance, or both) are strictly obeyed. The resonances in these orientations can be considered as almost perfect double resonances because both the incoming and the outgoing radiation have the same polarization and their frequencies display a difference of less than 0.7 meV, i.e., the two transitions start or end at the same CB or VB state (see Fig. 11). While the spin flip in allowed polarization has already been studied in Ref. 3, the resonance profiles have not been taken and the transitions in the forbidden Voigt geometry and in the Faraday geometry have not been observed previously. They are too weak in the off-resonance case for observation, but are strongly enhanced in resonance because of the double resonance of both incoming and outgoing radiation.

The positions of the observed resonances can again be attributed unambiguously to excitonic transitions. Details have been indicated in Fig. 6 and compiled in Table I. The agreement between observed values and those calculated from the luminescence experiments is definitely better in this case than for the allowed polarizations. Resonances for π- or σ-polarized radiation are found as expected from Fig. 2 with the exception of transition (3), expected at 1.819 eV, which cannot be traced reliably in the $-z(x,x)z$ spectrum. If present it should be smaller than resonance (d). The resonances in Fig. 6 are most remarkable because the amount of angular momentum, which is exchanged by the crystal with the radiation field during the scattering process, is either zero or two units $\hbar$, while m_S of the Mn^{2+} ground state changes by $\Delta m_S = +1$. This will be discussed in more detail below.

Forbidden resonances are also observed in the Faraday geometry, both in (σ^+,σ^+) and in (σ^-,σ^-) polarization (Fig. 8). A resonance, except of some spillover, is observed neither in (σ^+,σ^-) nor in (σ^-,σ^+) polarization. Again, as in Fig. 6, the resonances are stronger and their widths are reduced as compared to the allowed polarizations, and the selection rules for the polarizations are as expected from Fig. 2. Here the resonance (3) is occurring prominently in the (σ^-,σ^-) spectrum. Again, as in Fig. 6, the transfer of angular momentum between the photons and the crystal is zero, but the Mn^{2+} spin changes by $\hbar$.

IV. DISCUSSION

As the observed resonances of the scattering cross section are coinciding with the excitonic interband transitions (Table I), the experimental results presented above indicate that the nonlocalized excitonic band-edge states of the VB and CB are involved in the scattering processes considered here. This proves that for the spin flip of the Mn^{2+} ion an exchange process as indicated schematically in Fig. 9 has to be considered, in accordance with Ref. 3. It does not mean that excited localized $3d^5$ states are not

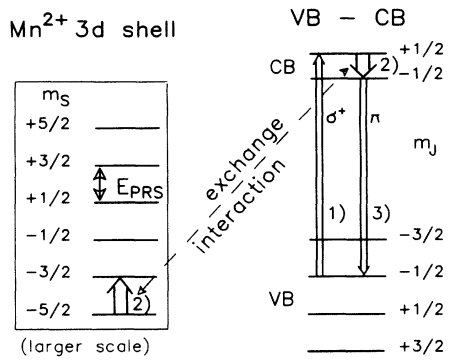

FIG. 9. Mechanism of Stokes scattering of PRS via exchange coupling between the spin of a CB electron and the electronic spin of a Mn^{2+} ion in its ground state (Ref. 3). σ^+ and π indicate virtual electric dipole transitions due to the incoming laser radiation (1) and the outgoing scattered radiation (3). Process (2) indicates the simultaneous spin flips of the electronic (CB) and the Mn^{2+} spins. A corresponding process can be constructed for a spin flip in the VB ["hole process"; see Eqs. (2) and (3), and Fig. 10]. The energy scales for the (Mn^{2+}) spin states and the electronic spins in the VB or CB differ by more than one order of magnitude.

participating at all in the scattering process. However, if such a $3d$ contribution exists ($E^{3d} \geq 2.3$ eV), it cannot be observed in our material with a small Mn^{2+} concentration because of the strong absorption due to the lower lying sp transitions at the band edge near 1.82 eV.

In the example depicted in Fig. 9 two excitonic band-gap states take part in the process as intermediate states (three step scattering mechanism): A virtual transition to the $m_J = +1/2$ CB state is induced by absorption of a σ^+ photon, followed by an electronic spin flip to the $m_J = -1/2$ state and subsequently by a virtual (or in

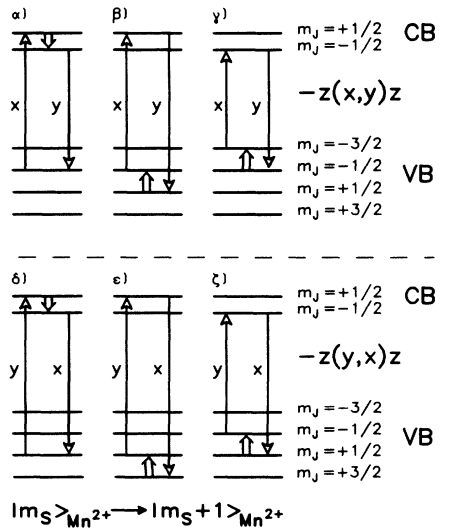

FIG. 10. Various possible virtual steps in the Raman scattering mechanism for allowed polarizations for the PRS (Fig. 5), involving transitions $\Delta m_J = -1$ of band electrons (α,δ) or holes (β,γ,ϵ,ζ). Case (α) has already been shown in Fig. 9 (from Ref. 3).

resonance real) recombination of the electron from the $m_J = -1/2$ (CB) state to the $m_J = -1/2$ (VB) state with π polarization. The virtual spin flip ($\Delta m_J = -1$) is coupled by the *sp*-3d exchange interaction with a spin flip $\Delta m_S = +1$ of the $3d^5$ shell. As a result of the process the orientational energy of the Mn^{2+} spin has increased by $2\mu_B B$ (μ_B is Bohr's magneton) and the electronic system has returned to its initial state. For more details see Ref. 3.

The exchange interaction between a Mn^{2+} ion and a CB electron or a VB hole is described by the following Hamiltonian (see references cited in Ref. 3):

$$H_{el} = \sum_n [J_e(\vec{r}_e - \vec{R}_n)\vec{S}_n \cdot \vec{s}_e + J_h(\vec{r}_h - \vec{R}_n)\vec{S}_n \cdot \vec{s}_h]. \quad (2)$$

Here $\vec{r}_e$, $\vec{r}_h$ and $\vec{s}_e$, $\vec{s}_h$ are the position and spin operators of electrons or holes, respectively, $\vec{R}_n$ and $\vec{S}_n$ refer to the nth Mn^{2+} ion, J_e and J_h are the exchange integrals, and

$$\vec{S}_n \cdot \vec{s}_e = S_n^z s_e^z + \frac{1}{2} S_n^+ s_e^- + \frac{1}{2} S_n^- \cdot s_e^+. \quad (3)$$

The shift operators $S_n^+ s_e^-$ and $S_n^- s_e^+$ result in

$$|m_S\rangle_n |m_J\rangle_e \rightarrow |m_S + 1\rangle_n |m_J - 1\rangle_e, \quad |m_S - 1\rangle_n |m_J + 1\rangle_e, \quad (4)$$

respectively.

We now concentrate on a more detailed discussion of the states involved in the scattering process. From Fig. 9 it is evident that for allowed (crossed) polarizations the CB or VB splittings are much larger than the energies of the PRS. Accordingly, only one of the intermediate states can be in resonance with the incident [ω_i coincides with the energy of the dipole transition in step (1) (Fig. 9): incoming resonance] or scattered light [ω_s coincides with transition (3): outgoing resonance] (see Table I). In the case of the parallel polarization double resonance is possible (see above), which reduces the spectral widths of the resonances.

In Fig. 9 only one scattering process has been shown schematically; others are equivalent and have been discussed previously by Petrou *et al.*[3] The various virtual transitions occurring in the VB and the CB, which can be conceived with respect to the allowed transitions in Fig. 5, are depicted in Fig. 10, following Ref. 3, and are compiled in Table I. Resonances (*a*) and (*b*), Fig. 5, can be interpreted (most probably) as the incoming and outgoing resonances of mechanism (β), which is a hole process (the virtual spin flip occurs in the VB). Resonance (*a*) may also be due to an electron mechanism (α). The outgoing resonance of (α) with π polarization and expected near 1.789 eV is not observed, but may be buried under the strong increase of the scattered intensity towards lower energies. As (*b*) occurs in an (x, y) spectrum, it must be interpreted as outgoing resonance of process (β).

Correspondingly, we interpret the resonances (*c*) and (*d*) again as incoming and outgoing resonances of process (ε), Fig. 10, but resonance (*c*) can also be attributed to the electron-process (δ). The outgoing partner of (δ), however, is expected near 1.82 eV (σ), but is again missing. All observed resonances may thus be attributed to hole processes only; however, electron spin flips in the CB may also contribute weakly. This is in agreement with the result of Gaj *et al.*,[13] where the ratio of the exchange integrals α/β of CB and VB electrons with Mn^{2+} has been determined to be -0.25. On the other hand, it should be taken into account, first, that the expected hole process (ζ) is completely missing here (its ingoing resonance might be covered by strong luminescence at 1.79 eV, however) and, second, that the in- and outgoing resonances (*a*) and (*b*) are separated only by 23 meV, but almost 30 meV are expected from the splitting of the light hole states in the VB at $B = 6$ T. The latter objection can be rejected considering Eq. (5), which describes the scattered intensity I_s for an incoming resonance at ω_{li}, full width at half maximum (FWHM) Γ_{li}, and an overlapping outgoing resonance at ω_{jk}, FWHM Γ_{jk}, neglecting effects due to alloy fluctuations and to the density of states:

$$I_s \sim \left| \sum_{k,l} \frac{M_{jk} S_{kl} M_{li}}{\left((\omega_L - \omega_{li}) - i\,\frac{\Gamma_{li}}{2}\right)\left((\omega_L - \omega_{\mathrm{PRS}} - \omega_{jk}) - i\,\frac{\Gamma_{jk}}{2}\right)} \right|^2, \quad (5)$$

where M_{jk} are the electric dipole transition matrix elements between states of the VB and the CB, S_{kl} is a matrix element of the *sp*-3*d*-exchange interaction, ω_L is the frequency of the incoming laser light, and $\omega_{li} = \omega_{jk} \pm \Delta V(\Delta C)$, where ΔV (ΔC) is the splitting in the VB (processes β, γ, ϵ, and ζ in Fig. 10) or in the CB (α, δ); $\omega_{li,jk}$ are the energy differences indicated by the arrows in Fig. 10. It is easily calculated that the observed resonance doublet displays a reduced frequency separation as compared to $|\omega_{li} - \omega_{jk}|$, in agreement with our result, if the observed Γ_{li} and Γ_{jk} are introduced in Eq. (5). In addition, if we compare the intensity of double resonances with a single resonance, where either the first or the second term resonates (incoming or outgoing resonance), we find a reduction of the single resonance intensity by two to three orders of magnitude. This compares well with the experimental data in Figs. 5, 6, and 8.

The resonances in forbidden (parallel) polarization (Fig. 6) are almost perfect double resonances, occurring between identical states with $\Gamma_{li} = \Gamma_{jk}, \Gamma_{li} \gg \omega_{\mathrm{PRS}}$. This is indicated by the large values of the intensities

attained. Under these circumstances the scattered intensity is maximum at $\omega_{res} = \omega_1 + 1/2\ \omega_{PRS}$ and the FWHM is reduced by roughly a factor $\sqrt{2}$ as compared to the single-resonance case, which is in agreement with the values given in Table I. Examples of the virtual transitions in and between the VB and the CB which may occur here are shown in Fig. 11. The most important contribution to the resonance (c) in the $-z(x,x)z$ spectrum is due to the (σ^+,σ^+) mechanisms (transition $|3/2,-1/2\rangle \leftrightarrow |1/2,+1/2\rangle$), labeled ($\alpha$), ($\beta$), and ($\gamma$) in Fig. 11. With these mechanisms one up- and one down-spin flip are connected with a total $\Delta m_J = 0$. Such a process will occur, if besides the Mn^{2+} spin there exists another spin excitation with an orientational energy undetectably small in Raman spectroscopy, but which balances the angular momentum and couples with the charge carriers either in the VB or the CB. This partner probably is a nucleus in the lattice which carries an angular momentum $I > 0$.

In Fig. 11 we have also plotted processes, which are singly resonant, i.e., which should contribute only a small intensity ($< 1\%$). These are the (σ^+,σ^-) or $(\Delta m_J = 2)$ processes with either transition 4 (Fig. 2) as an ingoing resonance and 6 as an outgoing resonance (ζ) or with 3 as an outgoing (σ^-) resonance (η); the latter is not observed. Other singly resonant processes are the (σ^+,σ^+) mechanisms (δ) and (ϵ), for which the second resonance is expected at transition 1, where it might be covered by the strong luminescence. In the lower part of Fig. 11 all possible virtual VB-CB transitions have been compiled concerning the (x,x) resonance at transition 6. The doubly resonant process (σ^-,σ^-) has contributions from spin flips both in the VB and in the CB (ι, κ). We cannot discriminate between these alternatives. Singly resonant processes [(σ^+,σ^-), (transitions 4,6; $\Delta m_J = 2$), (ζ)] or [(σ^-,σ^-), (6,3; $\Delta m_J = 0$), (λ, μ), not observed] should again play a minor role.

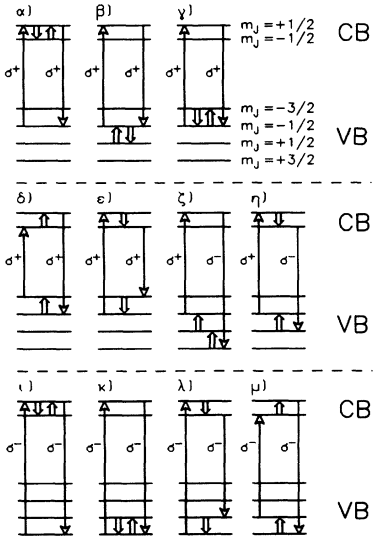

FIG. 11. (Upper part) Various possible virtual transitions in the forbidden ($\Delta m = 0$) doubly resonant transitions (σ^+,σ^+) (resonance c) in Fig. 6 (Voigt) and (a) in Fig. 8 (Faraday geometry); compare Fig. 10. Other doubly resonant processes with σ^- or π transitions behave accordingly. (Lower part) Examples of singly resonant processes (incoming or outgoing resonances) in forbidden polarizations.

The processes underlying the spectra taken in the Faraday orientation (Fig. 8) have already been treated by the examples given in Fig. 11 [(σ^+,σ^+), (4,4), (α, β, γ)]. Resonances at other transitions behave accordingly. Because of the strong resonance enhancement observed, doubly resonant processes are again prevailing here. Besides the (σ^-,σ^-) process (3,3), which is only observed in this polarization, there are in addition two singly resonant processes [(σ^-,σ^-), (6,3), (λ, μ, Fig. 11)] conceivable, where actually one of the spin flips induced by the charge carriers via exchange coupling should occur in the anti-Stokes spectrum.

In conclusion we can state that each of the forbidden spectra either in the Voigt or in the Faraday orientation can be interpreted by double-resonance processes, which agree with the strong increase of the observed scattered intensities. Only in a few cases singly resonant transitions may occur. In addition all forbidden transitions may be interpreted as ($\Delta m_J = 0$) transitions; only in a few exceptions ($\Delta m_J = \pm 2$) transitions may also contribute.

There appear three possible routes for an interpretation of the apparent "violation" of the angular momentum conservation in our experiments. First, the magnetic field along one of the cubic axes may intermix the free-ion wave functions of the ^6S multiplet in the ground state of $3d^5$ and the quantum numbers m_S are ill defined at $B > 0$. However, electron paramagnetic resonance (EPR) experiments in (Cd,Mn)Te or (Cd,Mn)S (Refs. 9, 10, 14, and 15) have shown that m_S is fully conserved because crystal-field effects are much smaller than the hyperfine interaction. In these EPR spectra the transition rules $\Delta m_S = \pm 1$ and $\Delta m_I = 0$ are strictly obeyed even at high fields. A second approach which has to be discussed here is the existence of spin clusters (exchange-coupled pairs, open and closed triplets, and more complex configurations of Mn^{2+} ions), which exist at the Mn^{2+} concentrations used in this work. The energy eigenvalues of pairs and triangles have been studied in detail.[16,17] Spin doublets display excitations energies at $2J_c$,$6J_c$,$12J_c$,..., where J_c is the Mn^{2+}-Mn^{2+} exchange constant in a Mn^{2+} complex. For a closed triangle energies at $3J_c$,$8J_c$,$15J_c$,... are found and for an open triangle $5J_c$,$7J_c$,$10J_c$,... have been computed.[16] The nearest-neighbor exchange constant J_c/k_b has been determined in (Cd,Mn)Te as (-6.2 ± 0.2) K for $x = 0.047$ (Ref. 18) and (-7.7 ± 0.3) K for $x = 0.05$.[19] If we assume for the present x value (0.135) a somewhat lower value ($|J_c/k_b| = 5$ K), we expect energies in addition to the PRS greater than 0.86 meV, which should be clearly resolvable in our experiment but which have not been observed. The exchange interaction of a single band electron (or hole) has been invoked in Ref. 4 to interpret the appearance of Raman PRS with $3\omega_{PRS}$, $4\omega_{PRS}$, and $5\omega_{PRS}$ in singly resonant [$(x,y),z$] spectra ($\Delta m_J = 1$), where angular momentum is also not conserved. The argument is, simply stated, that the local symmetry of an exchange coupled pair or triangle in a magnetic field

is generally lower than T_d or S_4, respectively; m_S is no longer a good quantum number due to the breakdown of rotational invariance and selection rules are accordingly relaxed.

These arguments do not apply in the interpretation of the present results, as the doubly resonant transitions in the forbidden polarizations are essentially ($\Delta m = 0$) transitions only and are in fact strictly allowed when point symmetry S_4 is applied. Even a single Mn^{2+} ion on a Cd site violates translational symmetry and lowers the site symmetry of the tetrahedrally bound Te ions next to it[20] because of a difference in bond strength between Mn-Te and Cd-Te. This reduction of symmetry does not induce, however, new magnetic resonance transitions in our spectra.

Larger clusters with larger Mn^{2+} distances and exchange constants J_1 ($< J$) will display a quasicontinuous energy spectrum[17] and may change their total angular momentum by one unit, but may contribute only a small amount of magnetic moment due to their complicated spin structure. If these large clusters were involved in the scattering process, we would expect an inhomogeneously broadened PRS, which is, however, also not observed. The width of the PRS remains narrow and the observed g factor is constant (Fig. 2) at all observed fields. So, as a third approach, it appears most probable that the magnetic nuclei in the lattice are involved in this scattering process. These nuclei are ^{55}Mn ($I = 5/2$, 100% abundance, $\mu/\mu_N = +3.469$), ^{111}Cd (1/2, 12.8%, -0.596), ^{113}Cd (1/2, 12.2%, -0.622) and ^{125}Te (1/2, 7.14%, -0.888), where μ is the magnetic moment of the nucleus and $\mu_N = eh/4\pi m_p$ is the nuclear magneton (m_p is the proton mass). The model sketched in Figs. 9 and 10 is extended to include a nucleus (^{55}Mn in Fig. 12), which interacts with the conduction electron of s-type symmetry via the contact interaction. The conduction electron performs two subsequent virtual spin flips between the $m_J = \pm 1/2$ states of the CB (Fig. 12). After the process the CB electron has returned to its initial state and the $3d^5$ spin and the nuclear spin both have altered their angular momenta by one unit in opposite sense [$\Delta(m_S + m_I) = 0$]. On the energy scale only the $3d^5$ spin flip counts because the nuclear orientation energy is too small to be traced in the Raman shift of the PRS. Evidently this scattering process gives rise to the observed double resonances, as $\omega_{PRS} \ll \Gamma_i$ (Γ_i is the half width of resonance i).

NMR experiments in (Cd,Mn)Te have been reported only recently.[20,21] ^{55}Mn, ^{113}Cd, and ^{125}Te NMR signals have been detected. It is found that the predominant interaction in nonconducting samples is the transfer hyperfine interaction of the Mn^{2+} ion with the Cd or Te nuclei. The shifts of the Cd and Te NMR lines due to this transfer interaction depend on the number of bonds separating the Mn ion from the Cd or Te ion. On the other hand, the shell-nucleus interaction in the ^{55}Mn ion gives rise to the prominent and well known hyperfine phenomena in the ESR spectra of Mn^{2+} compounds (compare Refs. 9, 10, and 25). No direct evidence for a hyperfine interaction between a CB electron and magnetic nuclei has been reported up to now in CdTe. However, this type of

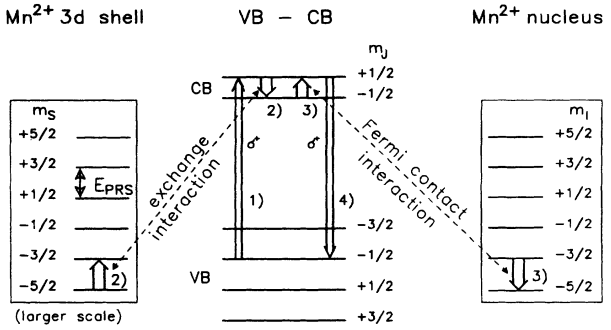

FIG. 12. Example of simultaneous interactions between virtual transitions of electronic spins in the CB (spin fluctuations) with the $3d$ shell of Mn^{2+} via exchange interaction and with the ^{55}Mn nucleus via contact interaction (6). $B > 0$, energies not in scale. If Cd or Te nuclei are involved ($I = \frac{1}{2}$), only two levels are found ($m_I = \pm\frac{1}{2}$) with $m_I = \frac{1}{2}$ being the lowest, because of the negative sign of the gyromagnetic ratio γ ($\sim \frac{\mu}{\mu_N}$, see text). The nuclear spin flip [arrow (3), right] occurs in the opposite direction.

interaction is well known in the isomorphous III-V compounds (e.g., in GaAs), where a whole research field has been established ("optical orientation" of electrons and nuclei[22,23]) and important applications have been developed. In fact, our experimental procedure of shining circularly polarized laser light on the sample in resonance with electronic transitions near the band edge is known to produce an easily detectable dynamic nuclear polarization in semiconductors without paramagnetic centers due to the generation of an effective magnetic field by the conduction electrons at the nucleus. The shift of the NMR frequencies due to this field is the Overhauser effect.

The hyperfine interaction due to the contact between s electrons (spin S) in the CB and nuclei with angular momentum I is

$$H_{HF} = A\,\vec{S}\cdot\vec{I}. \tag{6}$$

The hyperfine constant A is proportional to the probability of finding an electron at the nuclear site $\vec{r}_n$:

$$A = \frac{2}{3}\,\mu_0 g_B \hbar \gamma_n \left|\Psi(\vec{r}_n)\right|^2. \tag{7}$$

γ_n is the gyromagnetic ratio of the specific nucleus, g is the free-electron g factor, and $\Psi(\vec{r}_n)$ is the amplitude of the lattice-periodic part of the electron Bloch function at the site of the nucleus n.[24–26] Due to this interaction a very large nuclear polarization $\langle I_z\rangle$ beyond the thermal expectation value $\langle I_z\rangle_{\text{therm}}$ should be expected at high magnetic fields, where the paramagnetic fluctuations are suppressed, which otherwise increase the spin-lattice relaxation rate:

$$\langle I_z\rangle = \langle I_z\rangle_{\text{therm}}(1 + VS), \tag{8}$$

where S is the saturation parameter of the CB electrons [$0 \le S \le 1$, S large in (Cd,Mn)Te at high fields] and V is an enhancement factor

$$V = (g^* \mu_B)/(\hbar \gamma_n). \quad (9)$$

[g^* is the (very large) effective electronic g factor in semimagnetic (Cd,Mn)Te.[26]]

The p-type holes in the VB may couple by a magnetic dipole-dipole interaction, which, when decomposed into raising and lowering operators $S^{\pm}$ and $I^{\pm}$,[24,25] provides both simultaneous electronic and nuclear spin flips [Eq. (4)] and nuclear flips alone. This dipole-dipole interaction is generally weaker than the contact mechanism,[18] but the enhanced strength of the exchange integral of holes may partially compensate this deficit. Accordingly, the contribution of the hole processes depicted in Fig. 11 is not clear at the moment.

Now the Raman intensity [Eq. (5)] has to be extended to

$$I_s \sim \left| \sum_{k,k',l} \frac{M_{jk'} H^{\mathrm{HF}}_{k',k} S_{kl} M_{li}}{\left((\omega_L - \omega_{li}) - i\,\frac{\Gamma_{li}}{2}\right)\left((\omega_L - \omega_{\mathrm{PRS}} - \omega_{ki}) - i\,\frac{\Gamma_{ki}}{2}\right)} \right|^2, \quad (10)$$

where $\omega_{li} = \omega_{ki}$ and $\mathrm{H}^{\mathrm{HF}}_{k',k}$ is a matrix element of Eq. (6). Equation (10) clearly displays the double resonances for $\omega_L = \omega_{li}$ and the reduced half width; in the case of resonance it compares directly with Eq. (5) and the large intensity of the forbidden resonances can be understood considering the high density of states at k' even if $H^{\mathrm{HF}}_{k'k} < S_{kl}$.

This discussion can be summarized as follows.

Our results fully support the model of Petrou *et al.*,[3] which interprets the optically detected paramagnetic resonance signal as due to an exchange process with virtually excited electrons or holes in the CB or the VB (Fig. 10). The model has to be extended, however, by considering additional transitions (doubly resonant processes, Fig. 11), which give rise to forbidden resonances. These can be understood by considering a second partner involved in the PRS, which adds one unit of $\hbar$ but whose contribution to the magnetic moment is undetectably small in an optical experiment.

There are severe indications that the fluctuating spins in the system of the charge carriers both in the VB and the CB couple not only with the $3d$ shell by exchange interaction, but also with the magnetic nuclei via contact or dipole-dipole interaction. These fluctuations are induced by the resonantly excited optical transitions. The spectrum of the fluctuating exchange field or of the dipolar magnetic field comprises resonance frequencies both for electronic and nuclear transitions. In the allowed polarization only the electronic spin reorients; in the forbidden polarization a simultaneous flip of two spins $\Delta m = \Delta(m_S + m_I) = 0$ occurs (compare electron-nuclear double resonance measurements). Additional experiments, e.g., with varying concentration x, with improved spectral resolution and at high fields and in the anti-Stokes spectrum are desirable for further clarification.

Our results give evidence of the important role, that the magnetic nuclei can play in the semimagnetic compounds. It appears that such an influence has been, up to now, widely neglected in most discussions, e.g., of the magnetic polaron and of lifetime effects. A reconsideration of some arguments might be advisable in light of the results presented here.

V. RESONANCES OF THE PRS SIGNAL IN QUANTUM WELLS

The observation of the PRS in a quantum-well structure with $Cd_{1-x}Mn_xTe$ barriers and a CdTe well, where the gap E_0 at the Γ point in the barriers opens with growing x according to $E = (1.606 + 1.592x)$ eV at $T = 2$ K, adds some specific features to the problem.

(i) The degeneracy of light holes (LHs) and heavy holes (HHs) in the bulk material is raised and the resonances due to the LH and HH exciton transitions are expected to be separated by the effects of confinement and biaxial strain, which are different for LHs and HHs.

(ii) Furthermore separate luminescence frequencies are observed in the barriers and in the wells; the latter also depend on x because the tails of the excitonic wave function penetrate from the (diamagnetic) well into the semimagnetic barriers.

(iii) Due to the diffusion of the charge carriers from the barriers into the wells, the luminescence intensity at the frequencies of the barrier is drastically reduced as compared to the bulk in favor of the lower energies of the wells. Accordingly, Raman transitions covered under

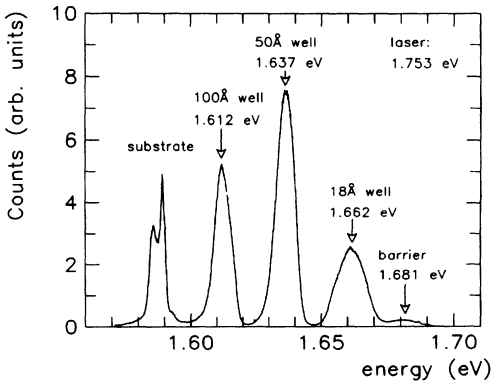

FIG. 13. Luminescence spectrum of a $Cd_{1-x}Mn_xTe/CdTe$ quantum-well structure with three different well widths. $x = 0.082$, $B = 6$ T, $\vec{B} \perp$ growth direction (Voigt geometry), and $T = 1.8$ K; the substrate is CdTe. Exciting field $\| \vec{B}$ and the polarization of luminescence is σ.

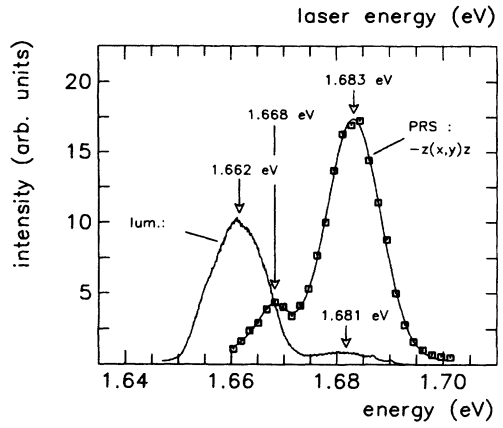

FIG. 14. Resonance of the PRS in allowed polarization (squares) and luminescence from the barrier and the 18 Å well in a quantum-well sample; the data are the same as in Fig. 13. The intensity scales differ for both plots.

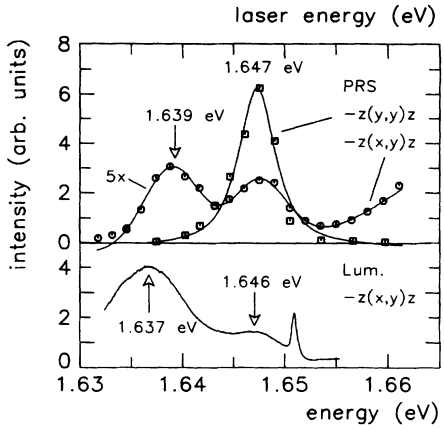

FIG. 15. Resonance of the PRS in allowed (circles) and forbidden (squares) polarization and luminescence in the region of the 50 Å well, showing light hole and heavy hole transitions. The forbidden (y,y) double resonance (different scale) only occurs in the light hole spectrum; the narrow line in the lower spectrum is the Raman signal from the electronic spin flip. Other data are the same as in Fig. 13.

the strong band-gap luminescence in the bulk material become observable in heterostructures.

We have used a quantum-well structure ($x = 0.090$) with three wells of different widths (Fig. 13). The structure was grown on a CdTe [100] substrate with a 200 nm CdTe buffer and 100 nm barriers of $Cd_{1-x}Mn_xTe$ between the wells. From photoluminescence excitation spectra (PLE) in the barrier $x = 0.0896 \pm 0.0012$ was determined. We have calculated the joint effects of lateral strain and confinement for the 50 Å well in this sample. We arrive at the same x, at an effective well width of 45.5 Å, and a VB offset of 10.5%. The centers of the split LH and HH VB states do not coincide. In Fig. 13 the luminescence spectrum for the exciting field along the direction of B (y, Voigt geometry) is depicted, showing peaks from the three wells, from the substrate and the barrier. In luminescence we expect the (2π) and (1σ) transitions (Fig. 2), which are observed at 1637 meV (HH) and 1646 meV (LH) (Fig. 15) at $B = 6.0$ T for the 50 Å well. The PLE maxima at $B = 0$ T are found at 1654 meV (HH) and 1667 meV (LH). Figure 14 shows an enlarged section of the luminescence and superimposed the Raman resonances of the PRS from the barrier and the narrowest well in (σ,π) polarization. In both cases there is a shift between the resonance and the luminescence peaks. Such shifts are also known from the electronic spin flip[11] in bulk material and could be interpreted quantitatively[11,12] to elucidate the nature of the intermediate state in this spin-flip Raman process. In the case of quantum wells the available data are less complete in this report at the moment. A full treatment has to await the results of further experiments. Figure 15 is a continuation of Fig. 14 to lower energies. In the lower half the two luminescence peaks due to light and heavy holes and the narrow Raman transition of the electronic spin flip in (σ,π) polarization are depicted; in the upper part the Raman cross sections of the PRS are shown both in allowed (σ,π) and in forbidden (π,π) polarization in the Voigt geometry. Light hole (2π) at 1647 meV and HH $(1\sigma$, 1639 meV) resonances are separated. As before the allowed resonances are broader ($\approx \sqrt{2}$) and weaker (≈ 10) than in the forbidden polarization, where a weak shoulder at 1655 meV, not visible in Fig. 15, is clearly indicating the double resonance (5π, LH, Fig. 2). The correlation of the resonances with the luminescence peaks is evident; obviously the LH transition at 1.646 eV corresponds to the decay of the LH free exciton. It is remarkable that the strong (π,π) resonance coincides with the LH exciton decay: The $(\Delta m = 0)$ transition (double resonance) is only possible between the CB and the LH in the VB.

ACKNOWLEDGMENTS

The authors are indebted to Dr. M. Dahl and Dr. J. Kraus (Würzburg) for valuable suggestions and to Dr. S. Gubarev (Chernogolovka), Professor H. Pascher (Bayreuth), and Professor I. A. Merkulov (St. Petersburg) for instructive discussions. The Deutsche Forschungsgemeinschaft has supported this investigation.

[1] S. Rodriguez and A. K. Ramdas, in *Highlights of Condensed-Matter Theory*, Proceedings of the International School of Physics "Enrico Fermi," Course LXXXIX, Varenna, 1983, edited by F. Bassani, F. Fumi, and M.P. Tosi (North-Holland, Amsterdam, 1985), p. 369; in *Light Scattering in Solids VI*, edited by M. Cardona and G. Güntherodt, Topics in Applied Physics Vol. 68 (Springer, Berlin, 1991), p. 137.

[2] J. K. Furdyna, J. Appl. Phys. **64**, R29 (1988).

[3] A. Petrou, D. L. Peterson, S. Venugopalan, R. R. Galazka, A. K. Ramdas, and S. Rodriguez, Phys. Rev. B **27**, 3471 (1983).

[4] D. L. Peterson, D. U. Bartholomew, A. K. Ramdas, and S. Rodriguez, Phys. Rev. B **31**, 7932 (1985).

[5] G. F. Koster, J. O. Dimmock, R. G. Wheeler, and H. Statz, *Properties of the Thirty-Two Point Groups* (MIT Press, Cambridge, MA, 1963).

[6] We apply the usual notation $a(b,c)d$, where a and d are the wave-vector directions of the incident and scattered light and b and d the polarization directions, respectively.

[7] W. Hayes and R. Loudon, *Scattering of Light by Crystals* (Wiley, Chichester, 1978), p. 254.

[8] Some care has to be taken when applying circular polarization of the incident and (or) scattered light in the Faraday orientation ($B \vec{\parallel} z$): Following the usual definition, in left (σ^+) or right (σ^-) circular polarization the electric field vectors E_L and E_R rotate in counterclockwise or clockwise directions when facing into the oncoming beam. A left-hand circularly polarized photon (σ^+) has a helicity $+\hbar$, and vice versa for σ^-. If the sense of rotation of the field is preserved when changing the direction of propagation ($\vec{k}_z \leftrightarrow -\vec{k}_z$), the helicity changes its sign. The transition operators in the dipole approximation for the absorption of a circularly polarized quantum of radiation is

$$\sigma^+, \sigma^- = \vec{r}^L, \vec{r}^R = \frac{1}{\sqrt{2}}(\vec{x} \pm i\vec{y}).$$

Thus the raising operator corresponding to $\vec{r}^L$ only forms nonvanishing matrix elements between an initial state with the angular momentum $n\hbar$ and a final state with $(n+1)\hbar$. In the case of the emission of a quantum $\sigma^\pm$ the operator $(\vec{r}^{L,R})$ applies and the initial state $n\hbar$ is connected to the state $(n \pm 1)\hbar$. Accordingly, the total angular momentum is preserved in every case. Thus, between levels of fixed angular momenta differing by $\hbar$, quanta of the same polarization σ^+ or σ^- are both emitted or absorbed. [For details see B. H. Bransden and C. J. Joachain, *Physics of Atoms and Molecules* (Longman Scientific & Technical, Harlow, 1983), pp. 175 and 213.]

[9] J. Lambe and C. Kikuchi, Phys. Rev. **119**, 1256 (1960).

[10] S. B. Oseroff, R. Calvo, W. Giriat, and Z. Fisk, Solid State Commun. **35**, 539 (1980).

[11] M. Hirsch, R. Meyer, and A. Waag, Phys. Rev. B **48**, 5217 (1993).

[12] R. Meyer, M. Hirsch, G. Schaack, A. Waag, and R.-N. Bicknell-Tassius, Superlatt. and Microstruct. **9**, 165 (1991).

[13] J. A. Gaj, J. Ginter, and R. R. Galazka, Phys. Status Solidi B **89**, 655 (1978).

[14] G. R. Wagner, J. Murphy, and J. G. Castle, Jr., Phys. Rev. B **8**, 3103 (1973).

[15] V. Ya. Bratus, I. M. Zaritsky, A. A. Konchits, G. S. Pekar, and B. D. Shanina, Fiz. Tverd. Tela (Leningrad) **18**, 2311 (1976) [Sov. Phys. Solid State **18**, 1348 (1976)].

[16] S. Nagata, R. R. Galazka, D. P. Mullin, H. Akbarzadeh, G. D. Khattak, J. K. Furdyna, and P. H. Keesom, Phys. Rev. B **22**, 3331 (1980).

[17] R. R. Galazka, S. Nagata, and P. H. Keesom, Phys. Rev. B **22**, 3344 (1980).

[18] D. Foner, Y. Shapira, D. Heiman, P. Becla, R. Kershaw, K. Dwight, and A. Wold, Phys. Rev. B **39**, 11 793 (1989).

[19] R. L. Aggarwal, S. N. Jasperson, P. Becla, and R. R. Galazka, Phys. Rev. B **32**, 5132 (1985).

[20] M. Bose, Phys. Rev. B **44**, 5343 (1991).

[21] K. Beshah, P. Becla, R. G. Griffin, and D. Zamir, Phys. Rev. B **48**, 2183 (1993).

[22] M. J. Dyakonov and V. I. Perel, in *Optical Orientation*, edited by F. Meier and B. P. Zakharchenya, Modern Problems in Condensed Matter Sciences Vol. 8 (North-Holland, Amsterdam, 1984).

[23] V. G. Fleisher and I. A. Merkulov, in *Optical Orientation* (Ref. 22).

[24] A. Abragam and B. Bleaney, *Electron Paramagnetic Resonance of Transition Ions* (Clarendon, Oxford, 1970).

[25] A. Abragam, *Principles of Nuclear Magnetism* (Clarendon, Oxford, 1982).

[26] W. Hofmann, H. Pascher, and D. Denninger, Semicond. Sci. Technol. **8**, 309 (1993).